DEVELOPMENT OF GLULAM MOMENT-RESISTING JOINT HAVING HIGH INITIAL STIFNESS, CLEAR YIELDING MOMENT AND RICH DUCTILITY

Kohei Komatsu[1], Tomohiro Morimoto[2], Shinsuke Kurumada[2], Hiroaki Tanaka[2]
Takeshi Shimizu[3], Shigeaki Kawahara[3], Nobuhiko Akiyama[3,4] , Makoto Nakatani[5]

ABSTRACT: Lagscrewbolt (LSB) has been used widely for composing glulam moment resisting column-leg as well as beam-column joints for constructing semi-rigid wooden frame structures. A serious problem on the existing LSB joint, however, was its brittle failure mode. In order to avoid this characteristic, Slotted Bolted Connection (SBC) systems, which is a kind of the friction damper for steel truss structure, was introduced to the existing glulam LSB joint system serially. Experiments on full-scale column-leg joint and beam-column joint, which were intended to be used in a three storey glulam school building, showed satisfactory performance on the requirements for the stiffness, yielding and ultimate performance. By this innovative investigation, a glulam semi-rigid portal frame, which has high initial stiffness, clear yielding capacity, rich ductility, and free from glulam brittle fractures, might be possible to be realized.

KEYWORDS: Glulam, Three storey school building, LSB, SBC

1 INTRODUCTION

Since the "*Act on the Promotion of the Utilization of Wood in Public Buildings*" [1] has been enforced on October 2010 in Japan, peoples' recognitions on constructing low-rise public buildings by using wooden materials seem to be increased positively year by year.

As timber materials, however, are not so stronger nor tougher than other conventional material such as steel, one of the most important and urgent issues for let public wooden buildings increase in Japanese society will be establishing reliable timber jointing technologies which are safety and robust against the attacks from devastating earthquakes without harming wooden members.

This research, therefore, aimed to develop glulam moment-resisting joints which have high initial stiffness, clear yielding moment and rich ductility and can be applied satisfactorily to the three storey school buildings which might be able to represent one of the large scale public wooden buildings in recent Japan.

1 Kohei Komatsu, RISH, Kyoto University, Japan
kkomatsu@rish.kyoto-u.ac.jp
2. Tomohiro Morimoto, Meiken Kogyou, Japan
t.morimoto@meikenkogyo.com
   Shinsuke Kurumada, Meiken Kogyou, Japan
shinsuke.kurumada@meikenkogyo.com
   Hiroaki Tanaka, Meiken Kogyou, Japan
hiroaki.tanaka@meikenkogyo.com
3.Takeshi Shimizu, Teco Two, Japan
t.shimizu@teco2.com
   Shigeaki Kawahara, Teco Two, Jpan
s.kawahara@teco2.com
4. Nobuhiko Akiyama, BRI, Japan
nakiyama@kenken.go.jp
5. Makoto Nakatani, Miyazaki Prefectural WURC, Japan
nakatani-makoto@pref.miyazaki.lg.jp

2 DESIGN TARGET

In order to make our research purpose be as clear as possible, we first set out our design target on a three storey school building, and used design loads assigned in the JIS-A3301 structural design standard for wooden school building [2]. JIS-A3301 standard, however, does not consider for constructing three storey school building, therefore, we selected a little bit rigorous structural design route in which allowable stress calculation method was necessary to meet with requirement of the relevant Japanese building codes [3].

Figure 1 shows a 3D-frame model of a three storey school building in which 6 class rooms of 8m by 8m plane area and 3m width corridors are involved. We assumed that ridge directional (X-direction) lateral resistance of the building is to be performed by the glulam semi-rigid portal frames, while that of span direction (Y-direction) is to be performed by any shear walls such as CLT or/and high-strength bracing system.
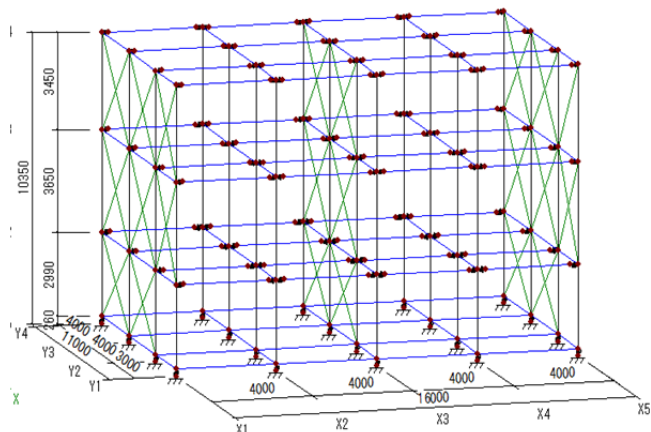

Figure.1 School building targeted in this research

3 OUTLINE OF STRUCTURAL DESIGN

3.1 ASUUMED LOADS

(a) Dead loads (JIS-A3301)
- Roof   1.1 kN/m²
- Floor   1.6 kN/m²
- External walls   1.3 kN/m²
- Internal walls   0.9 kN/m²

(b) Live loads (kN/m²) (JIS-A3301)

Place	Floor	Frame	Earthquake
Roof	0.49	0.30	0.20
Room, 1st, 2nd & 3rd floor	2.30	2.10	1.10
Corridor, 1st, 2nd & 3rd floor	3.50	3.20	2.10

(c) Snow load
- 0.60 kN/m² (snow fall depth : 30cm)

(d) Wind load (ridge direction)

Layer	Cumulative Area A_i(m²)	Wind factor C_f	Shear force Q_W (kN)
3	37.4	1.2	62.2
2	74.8	1.2	124.3
1	112.2	1.2	186.5

$Q_W = q \times A_i \times C_f$

q=1.385 kN/m² (max velocity: 36m/sec)

(e) Earthquake load (JIS-A3301)

Layer	w_i (kN)	Σw_i (kN)	α_i	A_i	C_i	Q_E (kN)
3	536.2	536.2	0.250	1.577	0.394	211.5
2	798.7	1335.0	0.623	1.213	0.303	404.7
1	808.4	2143.4	1.000	1.000	0.250	535.9

Design frequency: $T = 0.03H = 0.03 \times 10.35\text{m} = 0.3105\text{sec}$

$$\alpha_i = \sum_{j=i}^{n} w_j / \sum_{j=1}^{n} w_j , \quad A_i = 1 + \left(\frac{1}{\sqrt{\alpha_i}} - \alpha_i \right) \cdot \left(\frac{2T}{1+3T} \right)$$

$C_i = Z \times R_i \times A_i \times C_0 , \quad C_0 = 0.25$

$Z = R_i = 0$

$$Q_E = \sum w_i \times C_i$$

One of the most characteristic point of JIS-A3301 is that the base shear coefficient C_0 was assigned to be 0.25 which was a product of normal base shear of 0.2 times 1.25 as an "importance factor" for considering a bit higher safety for peoples in school class rooms.

3.2 ASUUMED MAIN STRUCTURAL MEMBERS

(a) Cross sections of column members

Storey	Width (y) (mm)	Height (x) (mm)	Code name
3rd	300	500	C3
2nd	300	550	C2
1st	300	640	C1

(b) Cross sections of beam members

Storey	Width (y) (mm)	Height (z) (mm)	Code name
3rd	180	600	GR
2nd	180	700	G2
1st	180	900	G1

(c) Mechanical properties of glulam member

Term	Value	Unit and Remarks
Species		Larch
Grade	E95F270	JAS standard [4]
Density	430	kg/m³
E_0	8.50	kN/m² AIJ [5]
E_{90}	0.34	kN/m² E_0/25 [5]
G	0.57	kN/m² E_0/15 [5]

(d) Strength of glulam member (E95F270)

Strength	F_c Compression	F_t Tension	F_b Bending	F_s Shear
	(N/mm²)			
Basic strength [*0]	21.6	18.6	27.0	3.6
Long-term allowable strength[*1]	7.92	6.82	9.90	1.32
Middle-short allowable strength[*2]	11.52	9.92	14.40	1.92
Short-term allowable strength[*3]	14.40	12.40	18.00	2.40

*0: Assigned by Architectural Institute of Japan [5]
*1: Long-term allowable strength=1.1/3×Basic strength
*2: Middle-short allowable strength=1.6/3×Basic strength
*3: Short-term allowable strength=2/3×Basic strength

3.3 ASUUMED MAIN STRUCTURAL JOINTS

(a) Specification and performance of Lagscrewbolt (LSB)

	LSBd25L450
Photo	
Place to be used	Parallel to the grain direction in the beam end joint and column end joint
Specification	Top diameter d_L : 25mm Bottom diameter d_{Lb} : 20mm Effective length L_e: 390mm Steel of LSB: S45C
Performance for Larch	Pull-out strength P_{0max} 124 kN Slip modulus K_{s0} 180 kN/mm

	LSBd30L640
Photo	
Place to be used	Perpendicular to the grain direction in the column side joint
Specification	Top diameter d_L : 30mm Bottom diameter d_{Lb} : 25mm Effective length L_e: 580mm Steel of LSB: S45C
Performance for Larch	Pull-out strength P_{90max} 117 kN Slip modulus K_{s90} 147 kN/mm

(b) Column-leg joint

Column-leg joint is composed of the serial system of a pair of glulam-LSB (4-LSBd25L450) joint and a pair of Slotted Bolted Connection (SBC) [5] with 3.5 mm thick brass shims in the interfaces of steel splice joint as shown in Figure 2. Shear resistance was taken by double 7-d16 drift pins. Detail of the joint is described in chapter **4**.
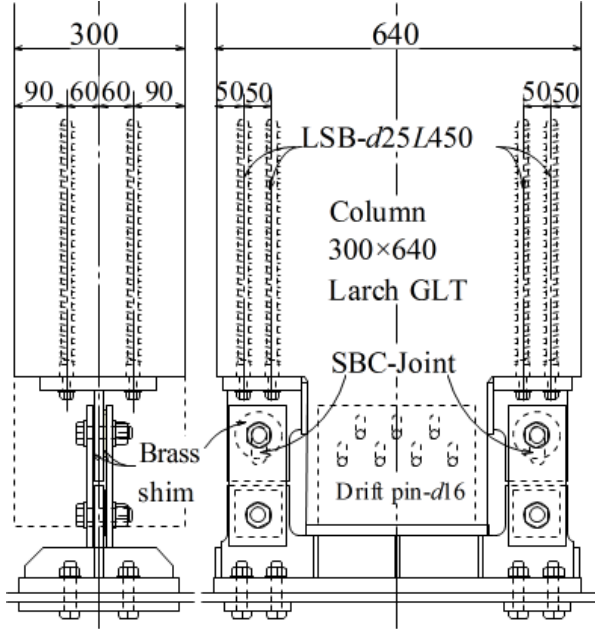

Figure 2 Outline of the column-leg joint.

(c) Beam-column joint

Beam-column joint is composed of beam-side joint which is basically same as column-leg joint and column-side joint. At column-side joint, a pair of 4-LSBd30L640 was used while for the beam-side joint a pair of 4-LSBd25L450 was used accompanying with a pair of SBC system [5] inserting 3.5 mm thick brass shims in the interfaces of steel splice joint as shown in Figure 3. Shear resistance was taken by double 15-d16 drift pined joint.
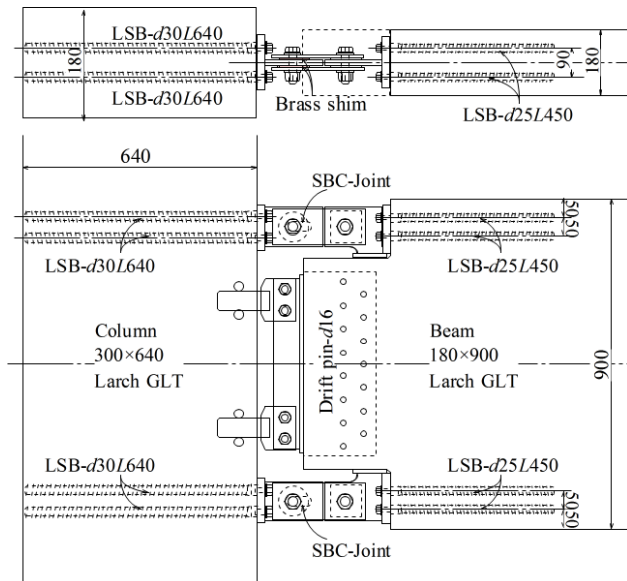

Figure 3 Outline of the beam-column joint.

(d) Rotational rigidity of joints for design calculation

Linear stress analysis was carried out on a 3D semi-rigid frame model (refer to Fig.1) using a commercial FEM program [6]. In the frame model, following rotational rigidities of beam-column joint as well as column-leg joint were used. Detail of the joint design is to be described in chapter **4**.

Table 1 Rotational rigidities

Location of joint	R_J (kNm/rad)
Beam-column joint at 3rd storey [*]	13320
Beam-column joint at 2nd storey [*]	19898
Beam-column joint at 1st storey	37000
Column-leg joint	29700

* Deduced from that of 1st storey beam-column joint

3.4 CHECK OF COMPUTED RESULTS

In this paper, only the computed results obtained in the case of earthquake load will be shown because in many cases such results tend to become the most critical in Japan.
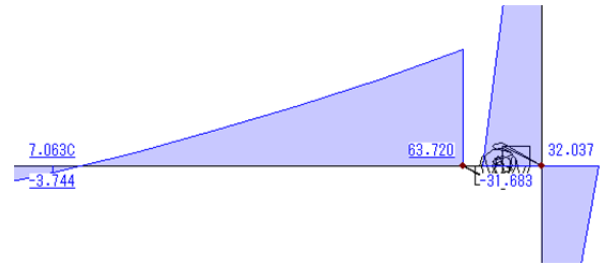
(a) Maximum stress on beam member

Figure 4 Maximum moment and axial force.

Maximum moment was observed at 2nd storey beam-column joint (Y2-X5-Z2 point in Fig.1) subject to dead load and live load assigned for earthquake loading condition, and following values were obtained.

$$M_{\max} = 63.72\text{kNm}, \qquad N = 7.063\text{kN},$$

The allowable strength check in a combined stresses situation is as follows [4].

$$\left(\frac{N}{A} \cdot \frac{1}{\eta \cdot f_c}\right) + \left(\frac{M}{Z_e} \cdot \frac{1}{f_b}\right)$$
$$= \left(\frac{7063}{180 \times 900} \cdot \frac{1}{0.977 \times 14.4}\right) + \left(\frac{63720000}{180 \times 900^2/6} \cdot \frac{1}{18}\right)$$
$$= 0.149 < 1 \quad \text{OK}$$

where

η : buckling reduction factor [4]

f_c, f_b : short-term compressive and bending allowable strength of Larch glulam (refer to 3.1-(d)), respectively.

3

(b) Panel shear at beam-column joint

The stress state in panel-shear zone of column-beam cross joint of glulam frame structure will be described like Figure 5 [6].
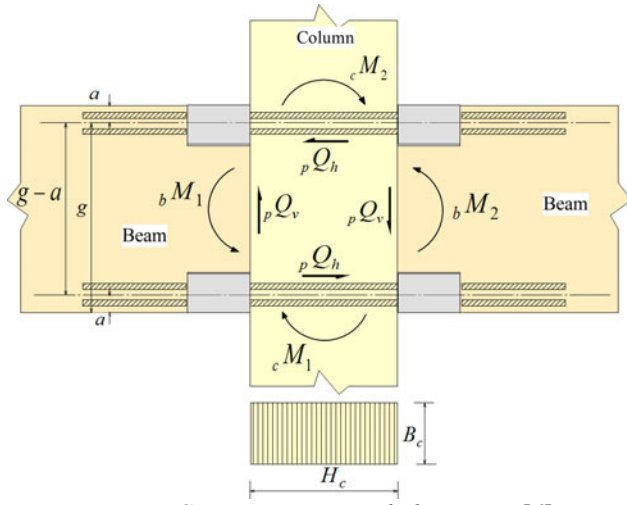

Figure 5 Stress state in panel-shear zone [6].

Stress components are expressed as equation (1) to (4).

$$_p\tau_v = \frac{_pQ_v}{B_c(g-a)} \le f_s \qquad ....(1)$$

$$_pQ_v = \frac{|_cM_1 - _cM_2|}{H_c} \qquad ....(2)$$

$$_p\tau_h = \frac{_pQ_h}{B_cH_c} \le f_s \qquad ....(3)$$

$$_pQ_h = \frac{|_bM_1 - _bM_2|}{g-a} \qquad ....(4)$$

From the stress analysis on a 3D frame structure subject to earthquake load, following stresses around panel zone of Y2-X4-Z2 point (refer Fig.1) were obtained;
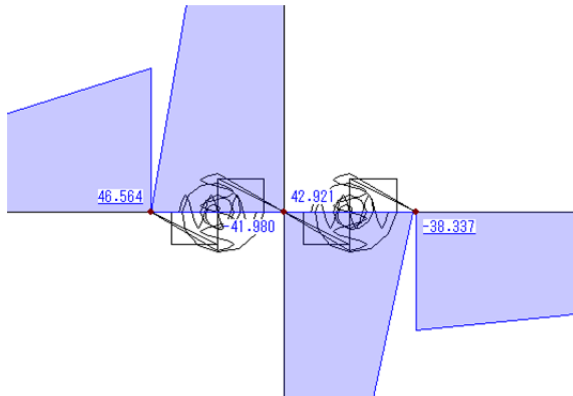

Figure 6 Moment distribution around panel zone.

$$_cM_1 = -41.980 \, \text{kNm} \,, \quad _cM_2 = 42.921 \text{kNm}$$
$$_bM_1 = 46.564 \text{kNm}, \quad _bM_2 = -38.337 \text{kNm}$$
$$H_c = 640 \text{mm} \,, \quad B_c = 300 \text{mm} \,, g-a = 750 \text{mm}$$

$$_p\tau_v = \frac{_pQ_v}{B_c(g-a)} = \frac{1000000 \times \dfrac{|-41.980 - 42.921|}{640}}{300 \times 750}$$

$$= \frac{132700}{225000} = 0.590 < f_s = 2.4 \text{N/mm}^2 \quad \text{OK}$$

$$_p\tau_h = \frac{_pQ_h}{B_cH_c} = \frac{1000000 \times \dfrac{|46.564 + 38.337|}{750}}{300 \times 640}$$

$$= \frac{113200}{192000} = 0.590 < f_s = 2.4 \text{N/mm}^2 \quad \text{OK}$$

Hence, criteria of panel shear stress were OK.

(c) Interlayer deformation angle

Figure 7 shows deformation diagram in Y2-ZX plane. Maximum inter layer deformation was observed at 2nd layer and its value was checked in accordance with [3]:

$$\gamma_{\text{max}} = \frac{28.09 - 11.06}{3650} = \frac{1}{214.29} < \frac{1}{200} \qquad \text{OK}$$
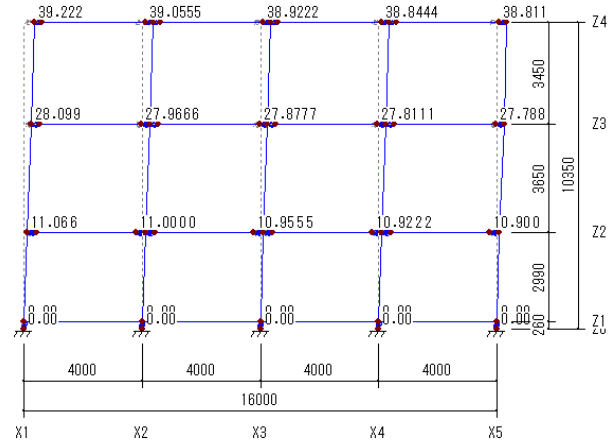

Figure 7 Deformation diagram of frame in Y2-ZX plane.

(d) Axial force on SBC system in column-leg joint

Maximum tensile force was observed in column-leg joint at X1-Y1-Z1point as shown in Figure 8.
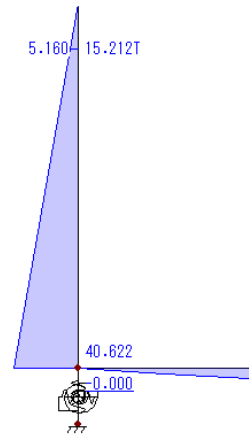

Figure 8 Column-leg joint where N_max was observed.

4

In this joint, both tensile force $N_{\max}/2$ due to axial force $N_{\max}$ and tensile force $F=M/g_a$ due to bending moment M act on SBC joint system as shown in Figure 9, thus the combined tensile force should be checked with initial slip capacity P_{slip} of SBC joint system.
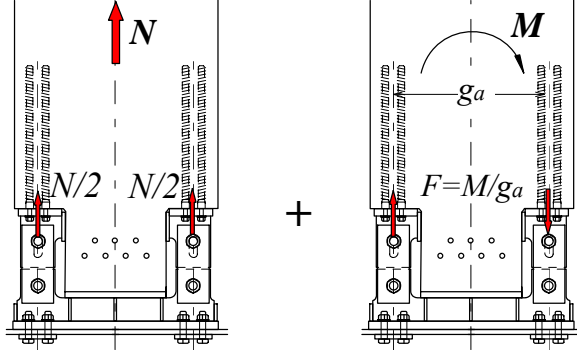

Figure 9 Tensile forces acting on the SBC joint system.

Computed results were as follows;

$$N_{\max} = 15.212\text{kN}, \qquad M = 40.622\text{kNm},$$

The initial slip load P_{slip} of the SBC joint system has been evaluated by the experiment [7] on the test specimens which had exactly the same profile as that of assumed SBC joint system in this article. The initial slip load P_{slip} can be estimated by equation (5) in accordance with the experimental result [7] and the high-tension bolt steel connection design manual [8]

$$P_{slip} = N \cdot \mu \cdot m \qquad \text{....(5)}$$

where

N : average bolt axial force induced =269(kN) [7]
m : number of friction surface=2
μ : coefficient of friction depending on surface treatment condition =0.38 (steel plates were all zinc galvanized) [7]

$$\frac{N_{\max}}{2} + \frac{M}{g_a} = \frac{15.212}{2} + \frac{40.622}{0.49}$$

$$= 90.51\text{lkN} < P_{slip} = 269 \times 0.38 \times 2 = 204\text{kN} \ \ \text{OK}$$

Hence, fundamental most structural design criteria were confirmed to be OK.

4 DESIGN CALCULATION OF JOINTS

4.1 COLUMN-LEG JOINT

Figure 10 shows a mechanical model of column-leg joint. Five serial springs along the tensile side, K_{LSB-0} , K_{uB} , K_{SBC} , K_{Steel} , and K_{lB} compose a resultant tensile rigidity of $_T K$ as shown in equation (6).

$$\frac{1}{_T K} = \frac{1}{K_{LSB-0}} + \frac{1}{K_{uB}} + \frac{1}{K_{SBC}} + \frac{1}{K_{Steel}} + \frac{1}{K_{lB}} \qquad \text{....(6)}$$

where,

K_{LSB-0} : slip modulus of tensile side LSB group

K_{uB} : elongation rigidity of upper connection bolts

K_{SBC} : shear slip modulus of smoother shim inserted into galvanized steel plate friction surface

K_{Steel} : axial rigidity of steel splice joint part

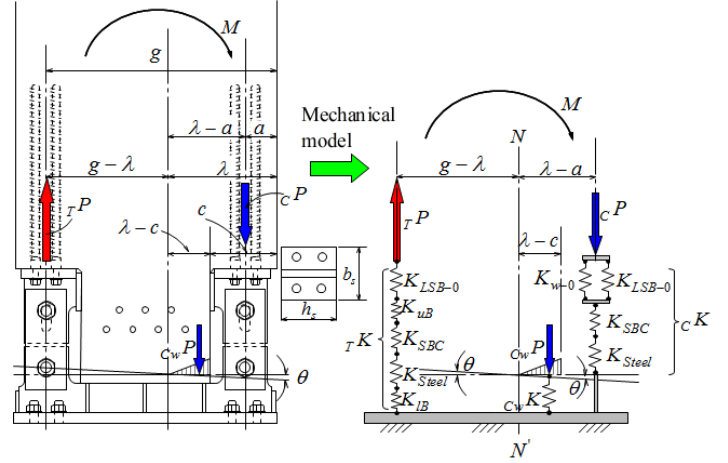K_{lB} : elongation rigidity of lower connection bolts

Figure 10 Mechanical model of column-leg joint.

While along the compression side, a pair of parallel springs K_{LSB-0} , K_{w-0} and serial springs K_{SBC} , K_{Steel} compose a resultant rigidity $_C K$ as shown in equation (7).

$$\frac{1}{_C K} = \frac{1}{K_{LSB-0} + K_{w-0}} + \frac{1}{K_{SBC}} + \frac{1}{K_{Steel}} \qquad \text{....(7)}$$

where,

K_{LSB-0} : slip modulus of compression side LSB group

K_{w-0} : parallel to the grain embedding rigidity of upper steel base which is estimated by equation (8).

$$K_{w-0} = k_{w-0} \cdot b_s \cdot h_s \ \ \text{(refer to Fig.10)} \qquad \text{....(8)}$$

where,

k_{w-0} : parallel to the grain embedment coefficient of timber which can be estimated by equation (9) through MOE of timber and contact depth b_s.[4],[6]

$$k_{w-0} = \frac{E_{w-0}}{31.6 + 10.9 \cdot b_s} \qquad \text{....(9)}$$

In addition to these, a resultant compression force $_{Cw}P$, caused by triangular contact stress distribution along the bottom part of column, is given by equation (10).

$$_{Cw}P = B \cdot \int_0^{\lambda-c} (k_{w-0} \cdot x \cdot \theta)dx = \frac{B \cdot k_{w-0} \cdot (\lambda-c)^2 \cdot \theta}{2} \text{...(10)}$$

From the Hooke's law of $_{Cw}P =\ _{Cw}K \cdot\ _{Cw}u$ that is held at the gravity point along the contact length of $(\lambda - c)$, equation (11) can be derived.

$$_{Cw}K = \frac{3k_{w-0} \cdot B \cdot (\lambda - c)}{4} \qquad ....(11)$$

By taking equilibrium equation among three axial forces, i.e. $_T P$, $_C P$ and $_{Cw}P$, we can determine the distance λ between most outer compressive edge to the neutral axis N-N' as shown in equation (12).

$$\lambda = \sqrt{\frac{1}{B \cdot k_{w-0}} \left\{ \begin{array}{l} \frac{1}{B \cdot k_{w-0}} \left(_T K +_C K - B \cdot k_{w-0} \cdot c \right)^2 \\ + 2 \left(_T K \cdot g +_C K \cdot a - \frac{B \cdot k_{w-0} \cdot c^2}{2} \right) \end{array} \right\}} - \frac{1}{B \cdot k_{w-0}} \left(_T K +_C K \right) + c$$

$$..(12)$$

Finally, from equilibrium among three force components and an external moment, we can get the rotational rigidity of the column-leg joint as shown in equation (13).

$$R_{J-cl} =\ _T K(g - \lambda)^2 +\ _C K(\lambda - a)^2 + \frac{B \cdot k_{w-0} \cdot (\lambda - c)^3}{3} \qquad ....(13)$$
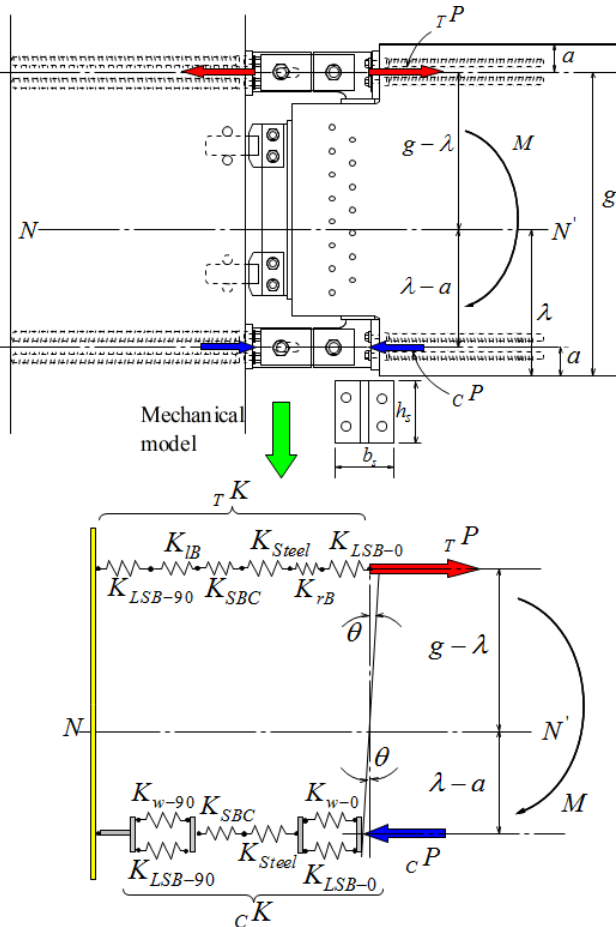
4.2 BEAM-COLUMN JOINT

Figure 11 Mechanical model of beam-column joint

Figure 11 shows a mechanical model of the beam-column joint. Six serial springs along the tensile side, K_{LSB-0}, K_{rB}, K_{Steel}, K_{SBC} K_{lB} and K_{LSB-90} compose a resultant tensile rigidity of $_T K$ as shown in equation (14).

$$\frac{1}{_T K} = \frac{1}{K_{LSB-0}} + \frac{1}{K_{rB}} + \frac{1}{K_{SBC}} + \frac{1}{K_{Steel}} + \frac{1}{K_{lB}} + \frac{1}{K_{LSB-90}}$$

$$....(14)$$

where

K_{rB}: elongation rigidity of right-hand side connection bolts

K_{lB}: elongation rigidity of left-hand side connection bolts

K_{LSB-90}: slip modulus of column side LSB group

On the other hand, six springs along the compression side, a pairs of parallel springs K_{LSB-0} and K_{w-0} corresponding to beam side, two serial springs K_{SBC}, K_{Steel} and a pairs of parallel springs K_{LSB-90}, K_{w-90} corresponding to column side, compose of a resultant compression rigidity $_C K$ as shown in equation (15).

$$\frac{1}{_C K} = \frac{1}{K_{LSB-0} + K_{w-0}} + \frac{1}{K_{SBC}} + \frac{1}{K_{Steel}} + \frac{1}{K_{LSB-90} + K_{w-90}} ..(15)$$

where

K_{w-0}: parallel to the grain embedding rigidity of right-hand side steel base which is be estimated by equation (8).

K_{w-90}: perpendicular to the grain embedding rigidity of left-hand side steel base which is be estimated by equation (16).

$$K_{w-90} = k_{w-90} \cdot h_s \cdot b_s \quad \text{(refer to Fig.11)} \qquad ...(16)$$

where

k_{w-90}: perpendicular to the grain embedding coefficient of timber $= k_{w-0} / 3.4$ [4]

By taking equilibrium equation between two axial forces, $_T P$ and $_C P$, we can determine the distance λ between most outer compressive edge to the neutral axis N-N' as shown in equation (17).

$$\lambda = \frac{_T K \cdot g +\ _C K \cdot a}{_T K +\ _C K} \qquad ....(17)$$

Finally, from equilibrium among two force components and an external moment, we can get the rotational rigidity of the beam-column joint as shown in equation (18).

$$R_{J-bc} = \frac{_T K \cdot _C K}{_T K +\ _C K} (g - a)^2 \qquad ....(18)$$

Consequently, the following initial rotational stiffness were obtained as shown in Tables 2 and 3.

Table 2 Rotational rigidity of column-leg joint

Term	value	unit	Remarks
K_{LSB-0}	741	kN/mm	4-LSBd25L450
K_{uB}	3141	kN/mm	4-F10T-M12-bolt
K_{lB}	5840	kN/mm	4-F10T-M16-bolt
K_{SBC}	1400	kN/mm	t=3.5mm brass shim
K_{Steel}	494	kN/mm	t=16mm & 9mm
K_{w-0}	92	kN/mm	b_s=140mm,h_s=120mm
k_{w-0}	0.0055	kN/mm^3	E_{w-0}=8500N/mm^2
R_{J-cl}	29699	kNm/rad	Column code name C1

Table 3 Rotational rigidity of beam-column joint

Term	value	unit	Remarks
K_{LSB-0}	741	kN/mm	4-LSBd25L450
K_{LSB-90}	716	kN/mm	4-LSBd30L640
K_{rB}	3141	kN/mm	4-F10T-M12-bolt
K_{lB}	3141	kN/mm	4-F10T-M12-bolt
K_{SBC}	1400	kN/mm	t=3.5mm brass shim
K_{Steel}	256	kN/mm	t=16mm & 9mm
K_{w-0}	92	kN/mm	b_s=140mm,h_s=120mm
K_{w-90}	27	kN/mm	b_s=150mm,h_s=120mm
k_{w-0}	0.0055	kN/mm^3	E_{w-0}=8500N/mm^2
k_{w-90}	0.0015	kN/mm^3	E_{w-0}=8500N/mm^2
R_{J-bc}	36955	kNm/rad	Code name C1-G1

4.3 YIELDING AND POST-YIELDING STAGE OF THE JOINTS

(a) Force-slip relationship of the SBC system
The force-slip relationship of the SBC system used in the column-leg and beam-column joint was determined independently by the experiment [7]. Obtained results were evaluated as shown in Figure 12 and Table 4.
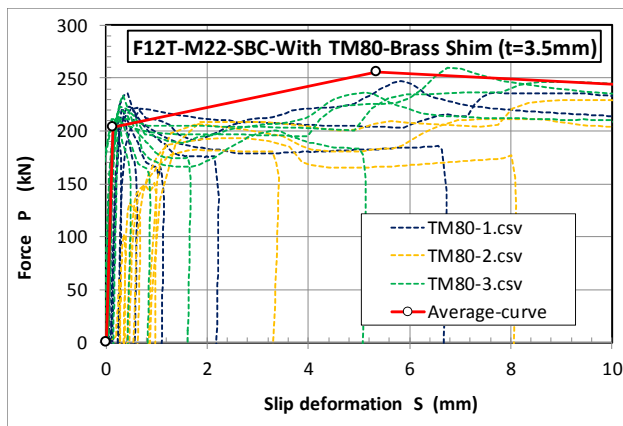

Figure 12 Evaluated test results of SBC system used.

Table 4 Tri-linear approximation of SBC system

Stage	Slip (mm)	Force (kN)	Rigidity (kN/mm)
1st Yield	0.146	204	1400
2nd Maximum	5.346	256	10
3rd Ultimate	30	194	-2.5

(b) Assumption on the ultimate (3rd) stage
Rigidity in the 3rd stage of the SBC system was estimated as minus value as shown in Fig.12 and Table 4. Minus spring constant, however, should not be used in the calculation of serial spring system, therefore, predictions of the joint performance in 3rd stage were executed by assuming that the rotational rigidity of the joints in 3rd stage was 10% of that of 2nd stage.

5 EXPERIMENTS

5.1 COLUMN-LEG JOINT

Figure 13 shows the test set-up of the column-leg joint specimen (C640). Right-down photo shows leg-steel parts already fixed to the reinforced H-shape steel beam. In the drawing of Fig.13, other measuring devices are removed for simplicity except those by whom rotational angle θ was estimated based on the following definition.

$$\theta = \frac{1}{2} \cdot \left(\frac{\#7-\#9}{h79} + \frac{\#8-\#10}{h810} \right) \text{ (rad.)}$$

Rotational moment θ at the column-leg joint was defined as shown in the drawing of Fig.13.

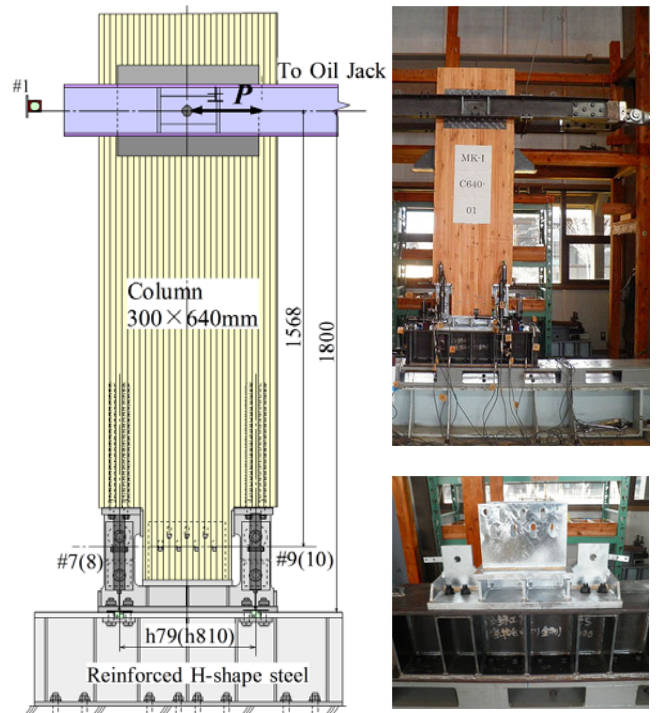$$M = 1.568\,(\text{m}) \times P\,(\text{kN}) \text{ (kNm)}$$

Figure13 Test set-up of the column-leg joint.

5.2 BEAM-COLUMN JOINT

Figure 14 shows the test set-up of the beam-column joint specimen (B900-C640). Figure 15 shows assembling process of the beam-column joint in an experimental laboratory. In the drawing of Fig.14, other measuring devices are removed for simplicity except those by whom rotational angle θ of the beam-column joint specimen was estimated based on the following definition.

$$\theta = \frac{1}{2} \cdot \left(\frac{\#9 - \#11}{h911} + \frac{\#10 - \#12}{h1012} \right) \quad \text{(rad.)}$$

Rotational moment M at the beam-column joint was defined as shown in the drawing of Fig.14.

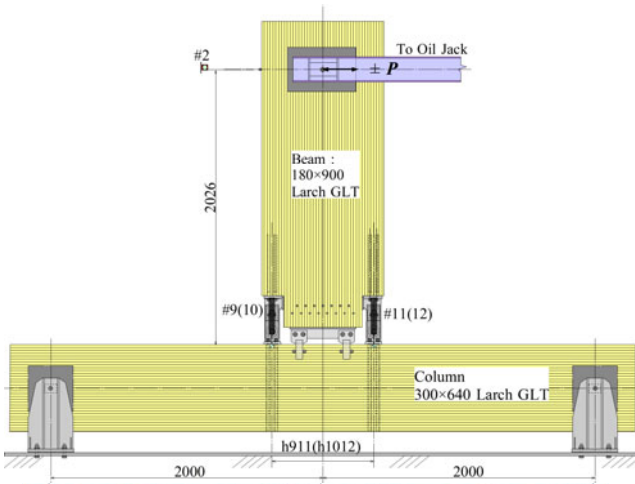$$M = 2.026\,(\text{m}) \times P\,(\text{kN}) \quad (\text{kNm})$$

*Figure14 Test set-up of the beam-column joint*

Figure 15 Assembling of the beam-column joint.

5.3 LOADING PROTOCOL

Static pull-push cyclic loadings were given to the test specimens in accordance with loading protocol so as to let the apparent shear deformation angle be $\pm 1/450$, $\pm 1/300$, $\pm 1/200$, $\pm 1/150$, $\pm 1/100$, $\pm 1/75$, $\pm 1/50$, $\pm 1/30$rad. Same shear deformation angle was repeated three times in each deformation level. Loading was started from "pull loading" and after reaching maximum load, loading was continued until load drops to 80% of the maximum load or deformation angle exceeds 1/15rad. Loading was stopped if load raised up suddenly due to contact of bolt shank to slotted hole end.

6 RESULTS & DISCUSSION

Figure16-(a), (b) and (c) show comparisons between observed moment-rotational angle relationships and predicted ones on the column-leg joint specimen.
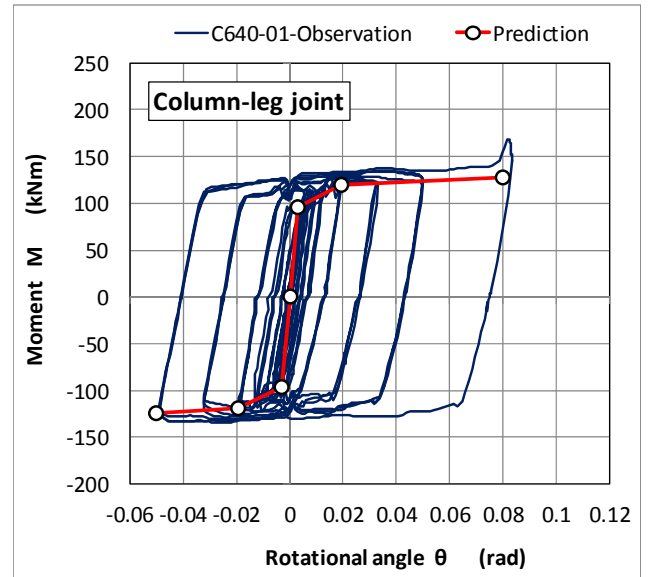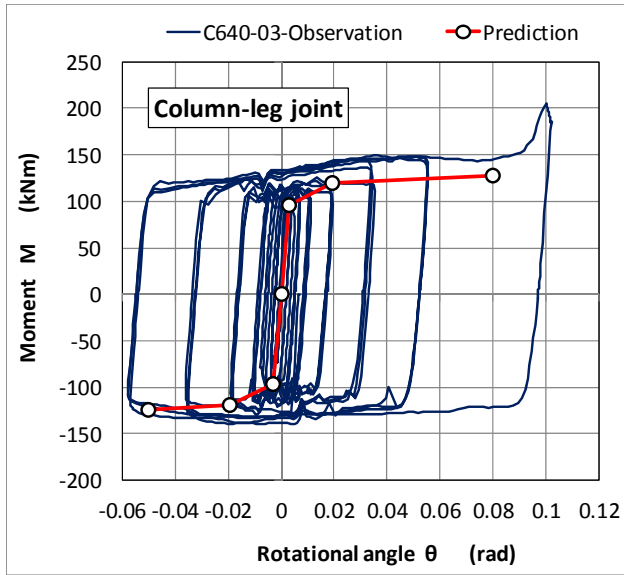

(a) $M - \theta$ relationship of C640-1
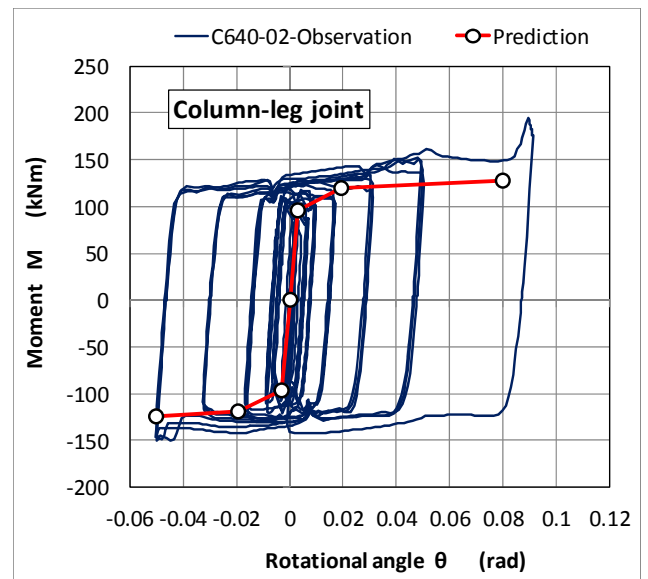
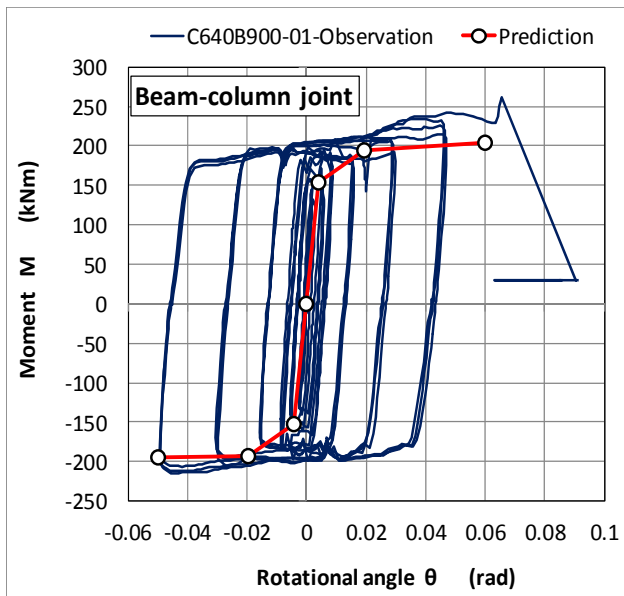(b) $M - \theta$ relationship of C640-2
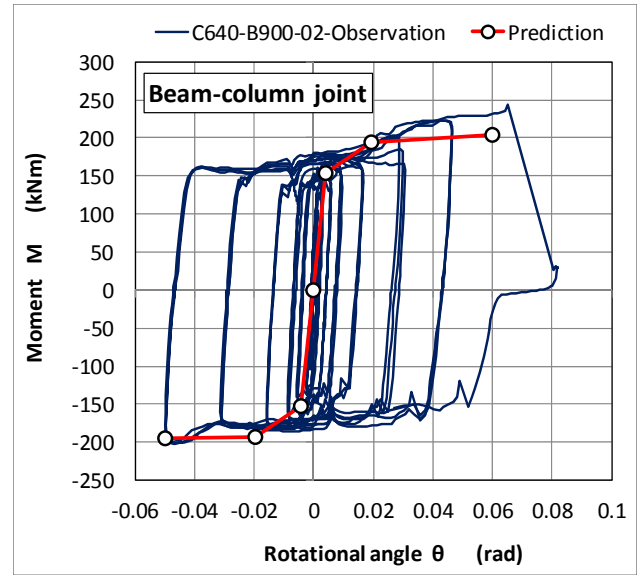
(c) $M - \theta$ relationship of C640-3

Figure 16 Comparisons between observed and predicted results on column-leg joint specimens

Figure17-(a), (b) and (c) show comparisons between observed moment-rotational angle relationships and predicted ones on the beam-column joint specimens.

From these comparisons, it will be confirmed that the design calculation method on LSB+SBC moment resisting joint system based on the mechanical models [9] can give not only precise predictions for the initial stiffness but also a little bit safety-side predictions for the yielding and ultimate load carrying capacities of the joint system.
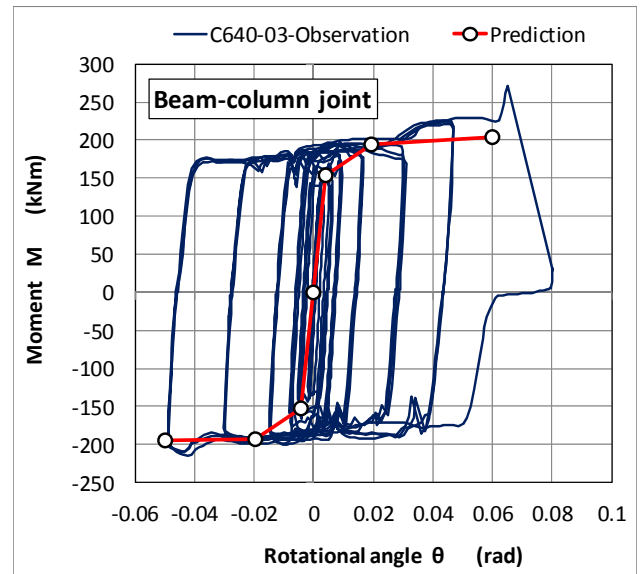
Figures 18 show some typical final phenomena of the column-leg joint specimens. Due to smooth sliding of M22 super high-tension bolt shank along the slotted hole, no glulam fractures were observed. Embedment of compressive steel plate was visibly observed.

(a) $M - \theta$ relationship of B900C640-1

(b) $M - \theta$ relationship of B900C640-2

(b) $M - \theta$ relationship of B900C640-2

Figure 17 Comparisons between observed and predicted results on beam-column joint specimens.
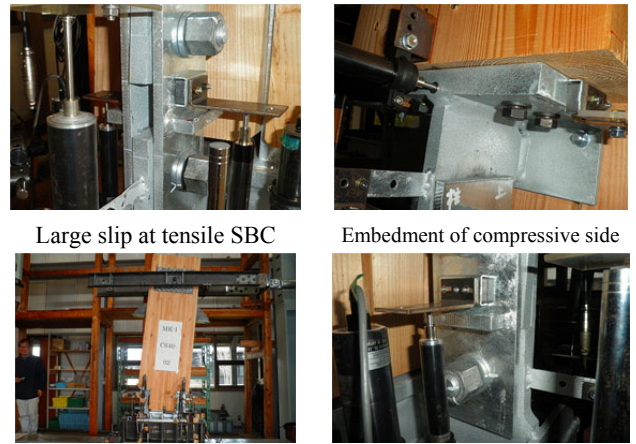

Large slip at tensile SBC   Embedment of compressive side

Large deformation   Contact of compressive SBC

Figure 18 Typical final phenomena of column-leg joint.

9

Large slip at tensile SBC · Tear-off of M12 connection bolts
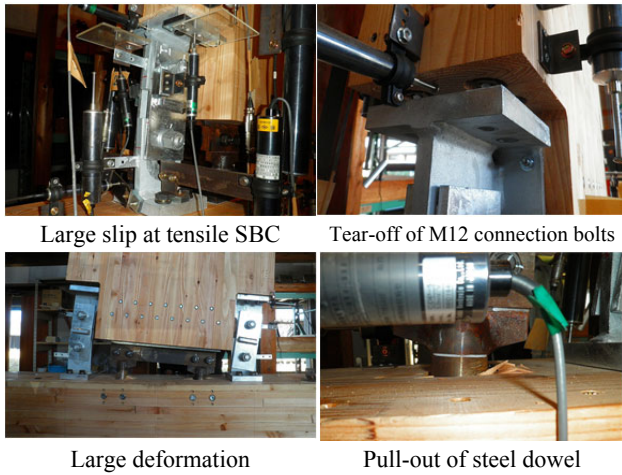
Large deformation · Pull-out of steel dowel

Figure 19 Typical final phenomena of beam-column join.

Figures 19 show some typical final phenomena of the beam-column joint specimens. Different from the column-leg joint, beam-column joint showed various non-fatal fracture phenomena such as pull-out of steel dowel from column side in the final stage (3rd stage) due to its relatively deformable connection characteristics between beam and column. Due to, however, smooth sliding of M22 super high-tension bolt shank along the slotted hole, no glulam brittle fractures were observed consequently. By the way, tear-off of M12 high-tension connection bolts were caused by the contact of M22 bolt shank to the end wall of slotted hole at final stage.
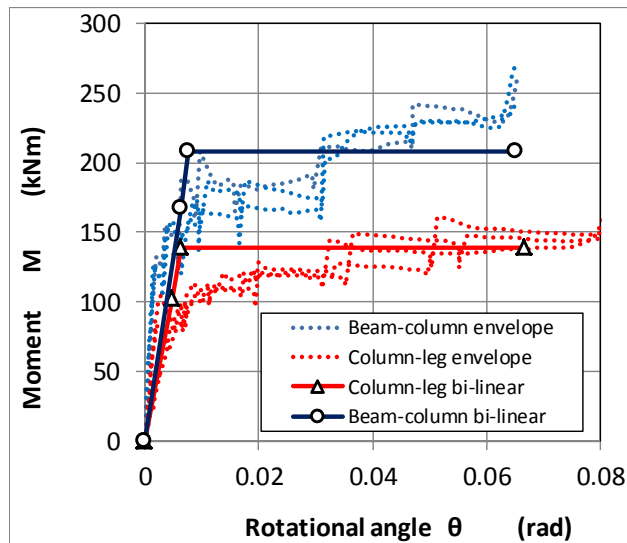

Figure 20 M-θ envelope relations and perfect bi-linear approximation of the data for both joint specimens.

Figure 20 and Table 4 and show evaluated results of the two types of joint specimen in accordance with the perfect bi-linear approximate method which is currently used mainly for evaluating shear wall performance [10].

From these evaluated results, it might be confirmed that column-leg joint showed a little bit richer on ductility factors than that of beam-column joint, but for the stiffness and ultimate moment capacity, inverse relationships were observed.

Table 4 Bi-linear approximation

Specimen	My	Mu	RJ	θy	θu	θv	μ
	kNm	kNm	kNm/rad	rad			
C640-1	108.6	125.1	23540	0.0046	0.0667	0.0053	12.56
C640-2	96.2	136.0	12996	0.0074	0.0667	0.0105	6.35
C640-3	103.6	157.0	45090	0.0023	0.0667	0.0029	23.00
Average	**102.8**	**139.4**	**27209**	**0.0048**	**0.0667**	**0.0062**	**13.97**
Standard deviation	6.2	16.2	16359				8.41
Lower 50%tile	99.9	131.7	19504				10.01
B900C640-1	213.3	187.6	26659	0.0070	0.0654	0.0080	8.18
B900C640-2	199.1	145.3	41095	0.0035	0.0650	0.0048	13.42
B900C640-3	212.6	167.6	20745	0.0081	0.0651	0.0102	6.35
Average	**208.3**	**166.8**	**29500**	**0.0062**	**0.0652**	**0.0077**	**9.32**
Standard deviation	8.0	21.1	10468				3.67
Lower 50%tile	204.6	156.9	24569				7.59

My : Yielding moment   Mu : Ultimate moment   RJ : Rotational rigidity
θy : Rotational angle at My   θu : Ultimate rotational angle
θv : Rotational angle at Mu

7 CONCLUSIONS

By introducing Slotted Bolted Connection (SBC) system into the existing Lagscrewbolted (LSB) glulam moment resisting joint system serially, a glulam semi-rigid portal frame, which has high initial stiffness, clear yielding capacity rich ductility, and free from glulam brittle fractures, might be possible to be realized.

REFERENCES

[1] Cabinet Order No.203 : Act on the Promotion of the Utilization of Wood in Public Buildings, October 2010. (in Japanese)

[2] JIS-A3301 : Structural design standard for wooden school building, revised on 27th March 2015. (in Japanese)

[3] Notification No.1899 and Article 82 of the Building Standard Law : Calculations of allowable unit stress, confirmation on interlayer deformation angle, eccentric ratio and so on, enacted by MLIT. (in Jpanese)

[4] Architectural Institute of Japan (edit.) : Standard for Structural Design of Timber Structures, Design data II, Marzen, 2006. (in Japanese)

[5] C.E.Grigorian, T.S.Yang and E.P.Popov: Slotted Bolted Connection Energy Dissipation, Earthquake Spectra, Vol.9, No.3, 491-504, 1993.

[6] ANON : Design Manual on Timber Joints by Lagscrewbolts (Ver.2.0), p.66, Japan Lagscrewbolt Society, October, 2015. (in Japanese)

[7] ANON : Friction joint test using 12G super high-tension bolt (SHTB) with varuous smooth sliping shims, Test report No.16-3540, Better Living Tsukuba Building Experimental Station, Feb., 2017. (Unpublished report) (in Japanese)

[8] Architectural Institute of Japan (edit.) : Recomendations for Design of Connection in Steel Structures, 3rd prints, 2012. (in Japanese)

[9] Takeshi Shimizu and Shigeaki Kawahara : Final report on the project of LSB+SBC system, April, 2017. (Unpublished report) (in Japanese)

[10] HOWTEC (edit.) : Allowable stress design for wooden conventional post & beam residential house, 2008. (in Japanese)